Civil Engineering Infrastructures Journal xx,xx

DOI: 10.22059/ceij.2026.390223.2247

Experimental and numerical studies on the behavior of GRP pipes subjected to strike-slip faulting in sandy soils

Alipouriani, M.R.[1], TahamouliRoudsari, M.[2]*,Moradi Garoosi, A.R.[2], Ghotb, M.R.[4]

1- Ph.D. student, Department of Civil Engineering, Kermanshah Branch, Islamic Azad University, Kermanshah, Iran.
2- Associate Professor, Department of Civil Engineering, Kermanshah Branch, Islamic Azad University, Kermanshah, Iran.
3- Assistant Professor, Department of Civil Engineering, Sanandaj Branch, Islamic Azad University, Sanandaj, Iran.
4- Assistant Professor, Department of Civil Engineering, Kermanshah Branch, Islamic Azad University, Kermanshah, Iran.

*Corresponding author, e-mail: me.tahamouli@iau.ac.ir

Orcids:

Mohammadraouf Alipouriani http://orcid.org/0009-0007-7634-7296

Mehrzad TahamouliRoudsari http://orcid.org/0000-0003-1069-3763

Allah Reza Moradi Garoosi http://orcid.org/0000-0003-1796-3623

Mohammad Reza Ghotb http://orcid.org/0000-0001-9449-2955

Received: 09/02/2025

Revised: 28/11/2025

Accepted: 10/01/2026

Abstract

Underground pipelines are vital infrastructures used for transporting energy and fluids. One of the primary seismic threats to these pipelines is fault displacement along their path. Therefore, investigating the behavior of these pipelines in various soil types under seismic effects is of significant importance. This study experimentally and numerically investigates the behavior of Glass Reinforced Polymer (GRP) pipes in dense and loose sandy soils subjected to strike-slip faulting. Initially, four experimental samples, including pipes with 100 mm and 200 mm diameters, were tested in dense and loose sand. Subsequently, numerical analyses were conducted to evaluate the effects of pipe diameter, pipe thickness, and pipe depth on the absolute displacement of the pipe at the failure moment. Additionally, the force causing the pipe failure was also calculated. The results showed that increasing the pipe diameter leads to more significant fault movement at failure. This effect is particularly pronounced in dense sand. Pipe strain and displacement changes were identified as reliable indicators for failure moments. The failure deformation of the pipe in loose sand was greater than in dense sand, such that the difference increased with a decrease in the pipe diameter.

Keywords:

Buried GRP pipelines, Finite element analysis, Pipe soil interaction, Dense sand, Loose sand

1. Introduction

The benefits of employing subterranean pipes for transportation include cheap transportation costs, low transportation loss, good safety performance, and minimal interference from the environment and climate change (Wang et al., 2020, Kliszczewicz, 2021). As a result, pipelines are now the primary means of transporting liquids and gases over great distances (Aghazadeh et al., 2025). Buried pipes, however, encounter various pavement regions and inevitably pass through numerous challenging areas, including cold and fault zones, frozen-thawed soil layers, and sandy soils (Liu et al., 2018b). The pipeline will experience some axial and shearing forces due to the fault. Internal deformation or relative movement creates interfacial stress between the pipeline and sandy soil, which has a more significant effect on pipeline safety (Tahamouli Roudsari et al., 2017, Liu et al., 2018a).

Several research efforts have concentrated on the challenges concerning the interaction between pipes and the surrounding soil. Vazouras et al. (2015) explored pipeline performance under permanent strike-slip fault movement using numerical simulations and closed-form solutions.

Considering finite and infinite lengths, they developed a force-displacement relationship for buried pipelines. The study highlighted the significant influence of end conditions, showing that local buckling occurs at small fault displacements. At the same time, excessive axial strains or cross-sectional flattening may cause failure as the fault angle increases. Dezhkam and Nouri (2018) introduce a mathematical model to assess the seismic response of water pipes embedded in soil subjected to far-fault earthquake loads. The study incorporates the Navier–Stokes equation to analyze fluid-pipe interaction, while the surrounding soil is modeled using spring elements. The research calculates dynamic deflection, revealing that buried pipes exhibit reduced deflection compared to those without soil support. Song (2006) conducted a thermal transfer analysis of a freezing soil medium containing an embedded pipeline. Xu et al. (2018) developed a numerical model to study pipe-soil interaction in horizontal directional drilling, highlighting the effects of radial displacement and soil wedging on pulling force predictions. Parametric studies revealed key factors influencing the wedging coefficient, improving prediction accuracy by up to 7.7% when accounting for soil and borehole characteristics. Ono et al. (2018) conducted two-dimensional simulations using a fluid-coupled discrete element method to analyze lateral loading on pipes buried in saturated sand. The study reproduced liquefaction through upward seepage effects, achieving accurate force-displacement curves. Contact force distributions and void ratio variations verified the method's applicability to pipe-soil interaction problems. Chaudhuri and Choudhury (2020) introduced a simplified analytical approach grounded in the Euler-Bernoulli beam theory to examine the impact of seismic landslides on buried continuous pipelines. They derived the differential equation of the pipe, modeled non-uniform ground deformations, and validated results against previous research. The study also conducted numerical analyses, revealing insights into pipe-soil interactions and deformation responses. Zhu et al. (2023) examined the mechanical response of X65 pipelines subjected to various traffic loads through field experiments. They developed a numerical model to capture the nonlinear pipe-soil interaction and implemented a dynamic vehicle load simulation. The study identified critical factors influencing axial stress and employed a machine learning model to predict pipeline responses, achieving high accuracy. Tahamouli Roudsari et al. (2022) introduced a novel method for evaluating the interaction between sandy soil and buried pipelines influenced by strike-slip faulting through two full-scale experiments on steel and polyethylene pipes. They utilized ABAQUS and an optimization algorithm to determine equivalent transverse spring stiffness, highlighting significant material dependence in pipe-soil interaction characteristics. Zhang and Askarinejad (2019) explored the soil-pipeline interaction within sloping grounds, focusing on the forces acting on buried pipelines due to soil instabilities. They developed a method to estimate ultimate external forces from slope failures using small-scale centrifuge tests on various sandy slopes. Their results highlight the impact of pipe burial depth and slope angle on pipeline stability. Soveiti and Mosalmani (2020) examined the performance of buried composite

pipelines subjected to strike-slip fault movements using nonlinear finite element analysis. Their study identified key factors influencing pipeline behavior, including pipe dimensions, composite lay-up, and soil stiffness. The findings emphasize the importance of optimizing the winding angle for improved engineering design and highlight the superior performance of composite pipes compared to traditional steel options. Research conducted on buried pipelines subjected to strike-slip fault movements includes the introduction of axial force terms to governing equations for buried pipelines (Talebi and Kiyono, 2020), the mechanical behavior of buried composite pipelines (Soveiti and Mosalmani, 2020), the performance of offshore pipelines (Triantafyllaki et al., 2021), the use of geofoam blocks for pipeline protection (Rasouli and Fatahi, 2020), and the failure analysis of large-diameter prestressed concrete cylinder pipelines (Li et al., 2022). Thang et al. (2022) explored the performance of double-wall steel–polymer–steel composite pipes under seismic conditions. They conducted a comparative analysis between single-wall and double-wall pipes in clay, finding that double-wall pipes exhibited improved resistance to displacement, strain, and stress. The study emphasizes the importance of bonding polymer to steel for enhanced structural performance.

Previous studies have rarely addressed the behavior of buried Glass Reinforced Polymer (GRP) pipes in dense and loose sandy soils. Additionally, the failure criteria and the soil-pipe interaction have received limited attention in both experimental and numerical studies. To bridge this gap, the present study examines the behavior of GRP pipes in dense and loose sand using both numerical and experimental approaches. The objective was to investigate the effect of pipe diameter, thickness, and burial depth on the pipe absolute displacement at failure and the applied force corresponding to failure in a strike-slip fault. The maximum force obtained from the analytical results was also compared with the ASCE guideline provisions, and a correction factor for the ASCE equation was proposed.

2. Test setup

The forces transferred to the pipe are a function of the deformation occurring in the pipe. Therefore, the dimensions of the box were selected so as not to affect the deformation of the pipe, ensuring that increasing the dimensions would not alter the results. For this purpose, extensive numerical studies were conducted using Abaqus software, which determined that dimensions of 1.5 × 1.5 × 8 meters for the box were appropriate. The box is composed of eight 1-meter sections and was installed in the structural research laboratory at the Islamic Azad University of Kermanshah. This box consists of two parts, one fixed and one movable, both having the same dimensions, as illustrated in Fig. 1. Steel wheels were installed beneath the movable section to facilitate its mobility. To prevent the fixed part from moving,

longitudinal stoppers were positioned, ensuring that its displacement remained nearly zero until the end of loading. All parts of this box were constructed from A36 steel and conservatively designed to withstand the applied forces.

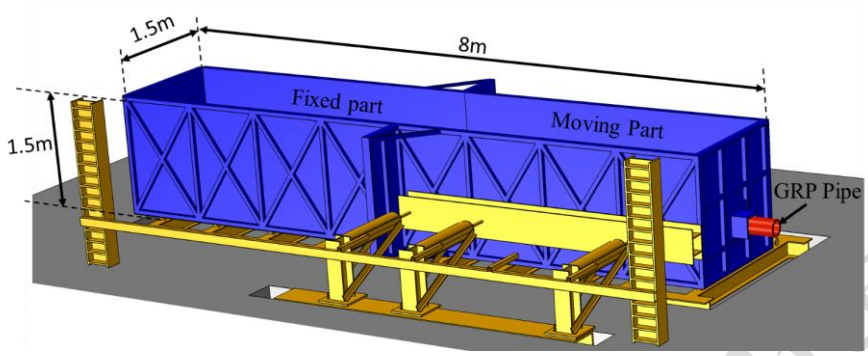

Fig. 1 Experimental setup

he loading was performed using a monotonic, displacement-controlled protocol. This approach enabled the application of uniform, incremental fault displacement, crucial for capturing the complete post-peak behavior of the pipe until final failure. Furthermore, the loading rate was maintained at a sufficiently low level to ensure quasi-static conditions, rendering dynamic and inertial effects negligible. A total of three 1050 kN hydraulic jacks were employed for applying force on the moveable part. A 32-channel data logger automatically managed the control of the jacks. Each hydraulic jack was fitted with a linear potentiometric transducer (LPT), with the system configured to ensure that the displacement discrepancy between the jacks remained under 0.5 mm at all times. The jacks were attached to rigid segments of the box structure, positioned at the same elevation as the buried pipe (Fig. 2(a)). Wires connected eight points along the pipe, spaced at intervals of 0.5, 1.5, ..., and 7.5 meters, to external LPTs, allowing displacement measurements with an accuracy of 0.2% throughout (Fig. 2(b)). These readings were used to determine the pipe's total deformation and its profile. A load cell was attached to each actuator to record and monitor the applied force at any moment. The pipe was centrally placed within the box, elevated 450 mm above the base, simulating a burial depth of 1 m. Caps were added to both ends to maintain the pipe's boundary conditions. The cap on the fixed end restricted longitudinal, lateral, and vertical movement, while the cap on the movable end restricted only lateral and vertical movement (Fig. 2(c)). Small gaps between the 1-meter pipe segments were sealed with plastic strips to prevent soil leakage. To detect the moment of pipe failure, the pipes were filled with water at a pressure of 2 bar. A pressure gauge, as shown in Fig. 2(c), was

used to monitor the internal water pressure at each loading step.

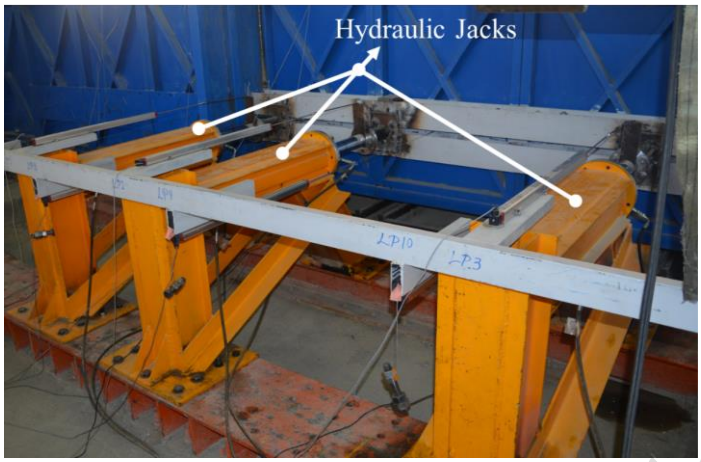

(a)

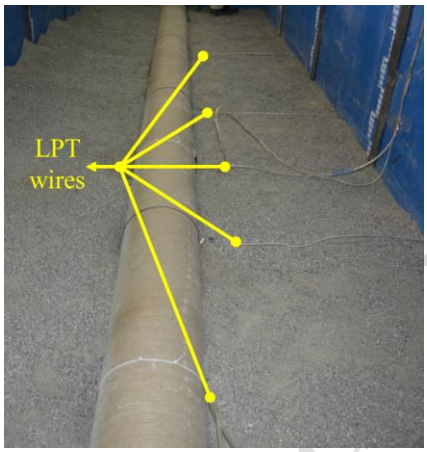

(b) (c)

Fig. 2 (a) Details of hydraulic jacks (b) Details of LPTs (c) Pressure gauge and pipe end connection

The experimental specimens consisted of four samples. The variables for these specimens included pipe diameter and soil type. The pipe diameters (D) were considered in two cases: 100 mm and 200 mm. The soil types in these models were defined as dense and loose sand. The specifications of these specimens are provided in Table 1. It is worth mentioning that the pipe material is identical in all four samples and is made of GRP.

Table 1 Specifications of experimental samples

Specimen	Type of sand	D (mm)	Pipe thickness(mm)
M-D200	Dense	200	4.9
M-L200	Loose	200	4.9
M-D100	Dense	100	3.5

M-L100	Loose	100	3.5

The specifications of the GRP pipes are based on a study by Tahamouli Roudsari et al. (2017). Both pipes were manufactured by the same company. Table 2 provides the material properties of these pipes. It is worth noting that the length of the pipes used in this study was 8.2m.

Table 2 Specifications of GRP pipe(Tahamouli Roudsari et al., 2017)

Property	Value
Poisson's ratio	0.3
Young's modulus (GPa)	12.91
Density (kg/m³)	2137

The soil utilized in the two models consisted of both dense and loose sand. This study employed Ottawa sand with a specific weight of 1660 kg/m³. The backfilling process beneath the pipe was carried out in two 200 mm thick layers, using a manual compactor to achieve the desired compaction level. Following this, the precise position of the pipe was determined, and displacement sensors were placed at 1-meter intervals. Subsequently, the soil above the pipe was filled in 200 mm layers until completion. Three samples were tested to evaluate the compaction level of each layer, and the average of these results was considered as the benchmark. The compaction properties of dense and loose sand layers are presented in Tables 3 and 4, as determined based on ASTM D3080 (2011). In this table, *Si* represents the i-th sample taken for the compaction test. Additionally, *L* and *D* represent loose and dense sand, respectively.

Table 3 Compaction percentages of dense and loose sand for a pipe with a diameter of 200 mm.

Layer	S1(D)	S1(L)	S2(D)	S2(L)	S3(D)	S3(L)	Average (D)	Average (L)
1	93	77	95	80	93	73	94	76.6
2	86	80	90	83	82	76	86	79/6
3	81	83	87	78/5	88	76	85	79.1
4	90	77	88	82	95	78	91	79
5	85	76	93	70	89	78	89	74.6
6	95	76	93	69	95	72	94	72.3

Table 4 Compaction percentages of dense and loose sand for a pipe with a diameter of 100 mm.

Layer	S1(D)	S1(L)	S2(D)	S2(L)	S3(D)	S3(L)	Average (D)	Average (L)
1	92	81.13	87	77.8	94	73	91	74.6
2	89	74	87	72	91	74	89	72.3

3	87.6	58	88	67	85	67.7	86.9	62.2
4	81	75	88	71.7	86	73	85	70.6
5	86	75	90	73.9	93	73	89.7	70.3
6	93	79.8	93	71.6	92	75	92.7	73.5

3. Results of experimental samples

This section focuses on the analysis of the experimental results. The hydraulic jacks were capable of applying a displacement of 600 mm. The loading of the models continued until the pipe failure occurred. The hydraulic jacks simultaneously applied displacement to the movable part of the model, and during the loading steps, the pressure inside the pipe was monitored. The condition of the upper sand layers in the model was photographed at each stage. Fig. 3 shows the deformation of one of the samples at four different displacement levels. These photographs were obtained by matching the moment of photography with the timing of the jack displacement application.

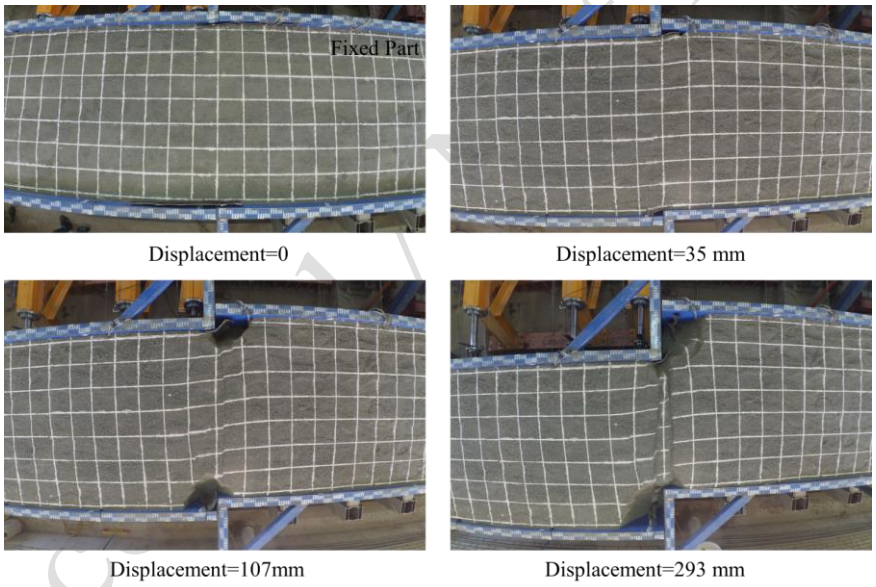

Fig. 3 Deformation of the sand during the loading of the M-L200 model.

At the end of loading the samples and the subsequent pipe failure, the sand was removed from the model to examine the pipe failure locations. It was observed that the failure regions in all models were almost identical and occurred in two specific sections, as shown in Fig. 4. These two sections were positioned on either side of the slip direction at an approximate distance of 0.4 meters from the boundary.

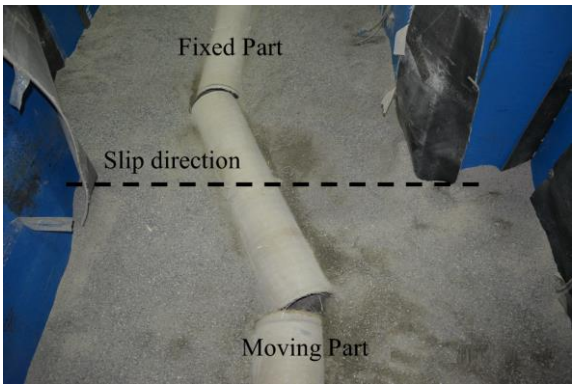

Fig. 4 Location of the pipe failure in the experimental specimens

In this section, the displacement of the pipe at the moment of failure was investigated. As previously mentioned, LPTs were placed one meter apart along the length of the pipe, and their labeling was done as shown in Fig. 5. It can be observed that points D1 to D4 are located in the fixed part, and points D5 to D8 are in the moving part.

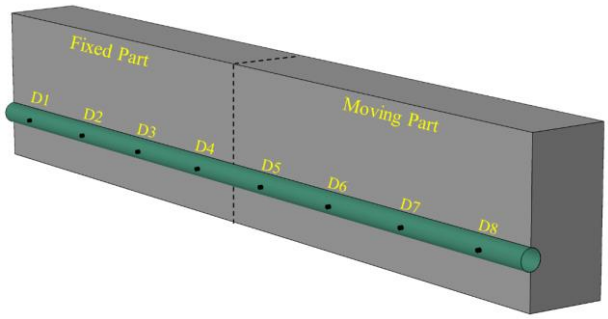

Fig. 5 Location of D1 to D8 sections in experimental samples

Fig. 6 illustrates the absolute displacement of the pipe at sections D1 to D8 at the moment of pipe failure. It can be observed that increasing the pipe diameter leads to an increase in the fault displacement corresponding to the pipe's failure moment. In dense sand, variations in pipe diameter have had a greater impact on the fault displacement corresponding to the pipe's failure moment. For instance, the displacement ratio of section D8 for ML-200 compared to ML-100 is 1.5, while this ratio for MD-200 compared to MD-100 is 2.9.

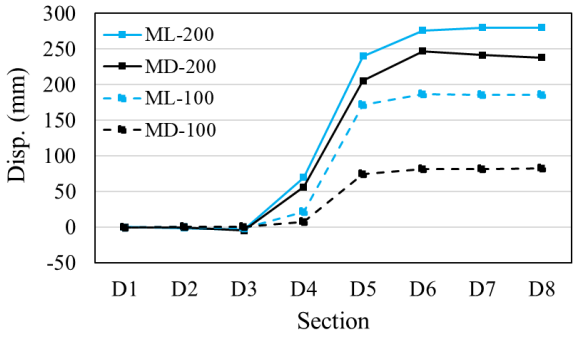

Fig. 6 Results of absolute displacement for the pipe in experimental samples

At the moment of pipe failure, the fixed part of the pipe tended to rapidly return to its initial state, meaning that the relative displacement with respect to the fixed part of the box decreased, with section D4 being the most affected. Thus, in addition to the internal pressure drop, the moment of failure could also be identified from the displacement curve of point D4. At the moment of pipe failure, along with the drop in displacement of point D4, the force applied by the hydraulic jacks also decreased. Fig. 7 presents the total force of the jacks versus the displacement of section D4 of the pipe. The red points in this figure indicate the moment of pipe failure. As observed, in all models, the moment of pipe failure is accompanied by a drop in both the displacement of point D4 and the applied force. The models with a pipe diameter of 200mm demonstrated higher displacement and experienced a more significant drop. A quantitative summary of the experimental results is presented in Table 5. In this table, Max disp. refers to the maximum absolute displacement of the pipe at the moment of failure.

As shown in Fig. 7, the 200 mm pipe develops higher forces in dense sand (MD-200) than in loose sand (ML-200). In loose sand, the pipe rests on a relatively soft support, so it can penetrate and move more easily inside the soil and the mobilised force remains limited. In dense sand, the soil behaves like a much stiffer support, the pipe penetration is restricted, and the imposed displacement is mainly resisted by pipe bending, which leads to higher force levels before failure.

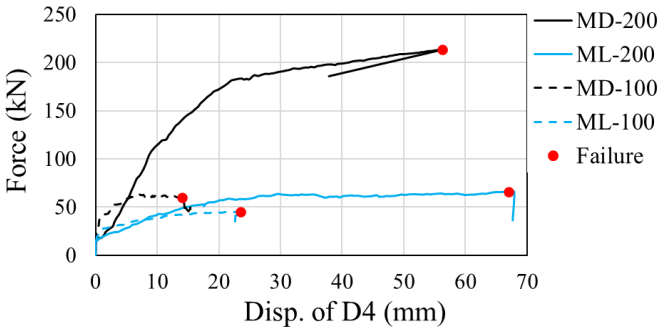

Fig. 7 Results of force versus D4 displacement

Table 5 Summary of experimental results

Specimen	Max disp. (mm)	Failure force (kN)
M-D200	247	213.46
M-L200	280	65.8
M-D100	83	65.78
M-L100	187	45.24

4. Numerical evaluations

Further numerical studies were conducted in this section to investigate the impact of pipe dimensions on its key parameters. For this purpose, the finite element software ABAQUS was utilized. Initially, the numerical model was calibrated using the results from experimental specimens, which are detailed in the following section.

4.1 Numerical model verification

An 8-node solid element (C3D8R) was used to model the sand. This element has three translational degrees of freedom at each node. To simulate the pipe, due to its thin thickness, a 4-node shell element (S4R) was employed. Each node of this element had three translational and three rotational degrees of freedom. The connection between these two elements was defined as a hard contact in the direction perpendicular to the pipe, and its contact connection was defined as a penalty method. Due to the large size of the model, the meshing was performed non-uniformly, with a mesh size of 80 mm at the furthest distance from the pipe and 20 mm near the pipe. Large deformations were considered throughout the model analysis. The loading was simulated by applying a monotonic lateral displacement to the movable section of the box. To fully capture the post-peak behavior and the failure mechanism of the pipe, a displacement-controlled protocol was adopted. This process was executed using the 'General Static' step in ABAQUS, ensuring quasi-static conditions and neglecting inertial forces, consistent with the experimental procedure. Fig. 8 shows the

boundary conditions of the meshed numerical model. The plastic behavior of the soil was modeled using the Mohr-Coulomb criterion (Hosseini and Roudsari, 2015), while the plastic behavior of the steel was defined based on the von Mises criterion with isotropic hardening (Cheraghi and TahamouliRoudsari, 2024, Cheraghi et al., 2024). After analyzing the numerical model, the results of the pipe deformation at the moment of failure were compared with the numerical results, as shown in Fig. 9. These results indicate that the numerical model provides a satisfactory level of accuracy.

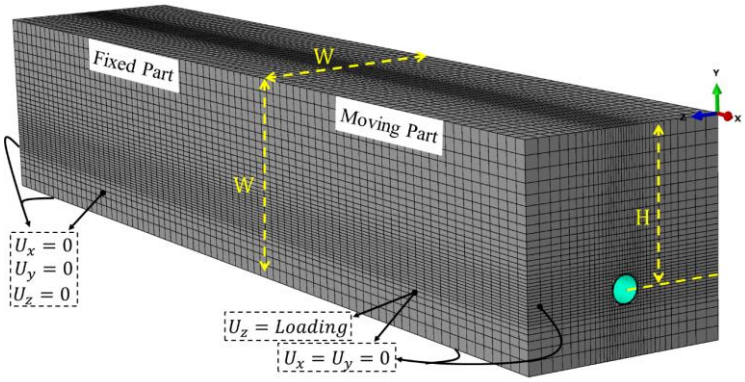

Fig. 8 Boundary conditions of the numerical model

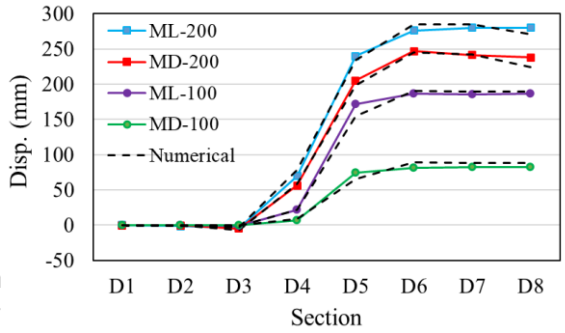

Fig. 9 Comparison of pipe displacement at failure: numerical vs. experimental models

After analyzing the numerical models, the logarithmic strain (LE) at the moment of pipe failure was extracted and is presented for four models in Fig. 10. As observed, the maximum strain in all results was calculated to be 0.015 and 0.016. Thus, these results can be considered as a criterion for the moment of pipe failure.

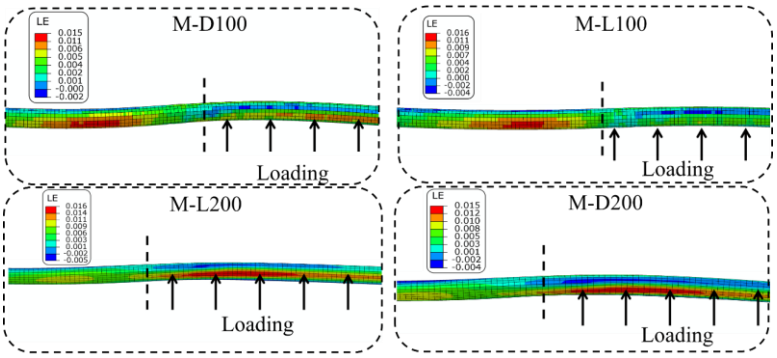

Fig. 10 The distribution of logarithmic strain at the moment of pipe failure.

Table 6 provides a more precise comparison of the numerical and experimental results. This table provides the applied force on the model at the moment of failure and the displacement of section D8. It is observed that there is a satisfactory agreement between the results.

Table 6 Comparison of experimental and numerical results

Models	Failure force (kN)		Disp. of section D8 (mm)	
	Exp.	Numerical	Exp.	Numerical
M-D200	213.46	223	238	224
M-L200	65.8	66.5	280	271
M-D100	65.78	66.9	83	88
M-L100	45.24	47.1	186	190

5. Parametric studies

In this section, parametric studies were conducted to investigate the variables affecting the behavior of the pipe. The models analyzed in this section were similar to the validation sample, differing in that three variables were considered. These variables included the diameter of the GRP pipe (D), its thickness (t), and the burial depth of the pipe (H), as illustrated in Fig. 8. These parameters were evaluated for both dense and loose sand. Consequently, all models analyzed in this section are summarized in Table 7. The models were labeled based on D and t. As previously mentioned, the dimensions of the steel box were designed to prevent any influence on pipes with diameters of 100 mm and 200 mm. Sensitivity analyses demonstrated that with box dimensions of 1.5×1.5×8 meters, the pipe deformation results remained unaffected by the box size. However, an increase in pipe diameter necessitates a proportional increase in box dimensions to maintain this condition. Therefore, for pipe diameters exceeding 200 mm, the box dimensions were increased to 3×3×8 meters. Additionally, the diameter-to-thickness ratios of the models were categorized into three levels: 50, 25, and 12.5.

Table 7 Dimensions of the parametric models.

Models	D(mm)	t(mm)	D/t	W(m)	H(m)
M-100-2	100	2	50	1.5	1
M-100-4		4	25		
M-100-8		8	12.5		
M-150-3	150	3	50		
M-150-6		6	25		
M-150-12		12	12.5		
M-200-4	200	4	50		
M-200-8		8	25		
M-200-16		16	12.5		
M-250-5	250	5	50	3	2
M-250-10		10	25		
M-250-20		20	12.5		
M-300-6	300	6	50		
M-300-12		12	25		
M-300-24		24	12.5		
M-350-7	350	7	50		
M-350-14		14	25		
M-350-28		28	12.5		
M-400-8	400	8	50		
M-400-16		16	25		
M-400-32		32	12.5		

The analysis of the models continued until the LE of the pipes reached 0.0155. Then, the absolute deformation of the pipe at the moment of failure, as well as the force applied to the model at this moment, were calculated.

The results of the absolute deformation of the pipe at the moment of failure are presented in Figs. 11 and 12, corresponding to loose and dense sand, respectively. It is noteworthy that although the loading protocol applied to the steel box wall (the soil boundary) was uniform and displacement-controlled for all sections D5 to D8 in both numerical and experimental models, the recorded displacements in these sections (Figs. 11 and 12) represent the absolute displacement of the pipe resulting from the Pipe-Soil Interaction (PSI) and the pipe's axial and flexural stiffness. Due to the relative deformation of the pipe within the soil medium, the displacement in these pipe sections is non-uniform, and the pipe did not experience a uniform displacement. By analyzing the results, it is observed that this non-uniformity is directly related to the pipe stiffness; such that in models with larger diameter and thickness (higher stiffness), the displacements of sections D5 and D8 are closer to each other. This indicates that an increase in pipe stiffness leads to a nearly rigid behavior of the pipe in the fault zone and makes the displacement distribution in the movable section more uniform.

As observed, an increase in deformation, as well as pipe diameter and thickness, leads to greater deformation at the moment of failure. Across all results, the displacements of

sections D6 to D8 were approximately identical. Meanwhile, the deformation of steel pipes at sections D7 and D8 was nearly identical (Tahamouli Roudsari et al., 2022). Due to the lower stiffness of GRP pipes compared to steel pipes, deformation is concentrated primarily at the middle and near the fault. Consequently, the curvature of the GRP pipe is more pronounced in sections closer to the fault.

A comparison of the results for models with dense and loose sand indicates that the displacement required for pipe failure in loose sand was greater than in dense sand. Due to the lower stiffness of loose sand compared to dense sand, the curvature of the pipe near the fault is reduced. In loose sand, pipe deformation is distributed over a greater length, whereas in dense sand, it is concentrated over a shorter length. Consequently, the curvature near the fault is greater in dense sand, leading to a lower displacement required to cause pipe failure in dense sand. Furthermore, as the pipe diameter decreased, the difference in results became more pronounced. For instance, the displacement required for pipe failure in model M-100-8 was 201 mm in loose sand and 94 mm in dense sand. Conversely, for model M-400-32, the displacement required for pipe failure was 489 mm in loose sand and 437 mm in dense sand.

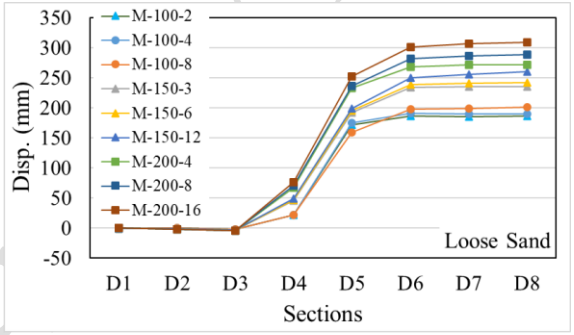

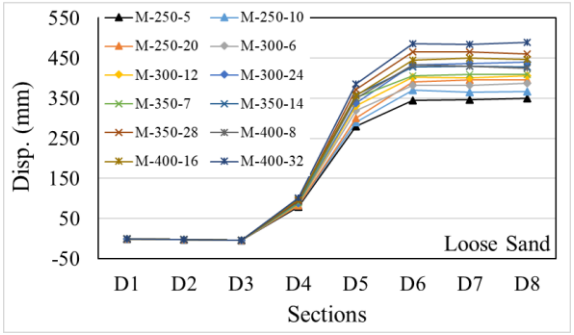

Fig. 11 The absolute deformation of the pipe at the moment of failure in loose sand.

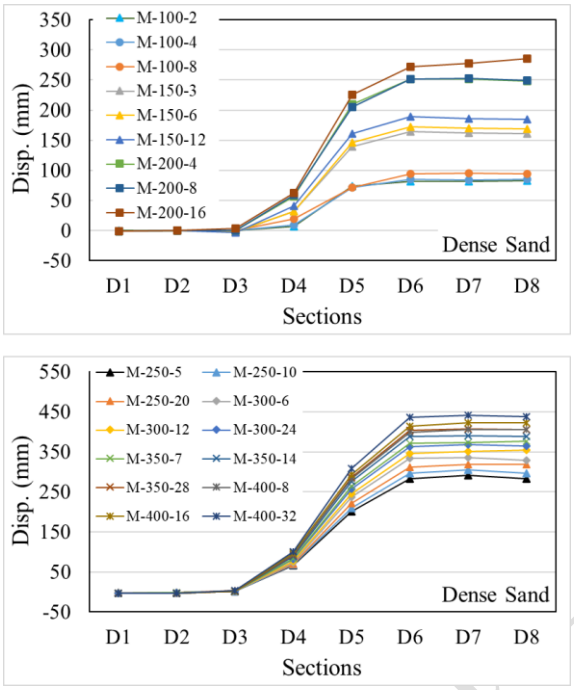

Fig. 12 The absolute deformation of the pipe at the moment of failure in dense sand.

The deformation results presented in Figs. (9, 11, and 12) indicate that the pipe displacement (i.e., at D4) is not zero. This occurs because the movement at section D5 initiates the pipe's bending and deformation, and these forces are then transferred axially and flexurally toward the fixed end, ultimately resulting in the displacement observed at D4.

A crucial finding is that the displacement at D4 is greater in loose sand compared to dense sand. This difference is attributed to the lower stiffness and confinement of loose sand, which allows the pipe to deform and penetrate the soil more easily. This mechanism causes the axial forces to propagate over a greater length of the pipe, resulting in a larger accumulated displacement at section D4 before failure.

The distribution of strain at the moment of failure was examined in this section. Fig. 13 presents the logarithmic strain results for several models in the fault zone. This strain distribution corresponds to the final moment, i.e., pipe failure. To more precisely identify the location of maximum strain, these models are presented without deformation. In these models, it can be observed that the distance of maximum strain from the fault direction is nearly identical across all models. It is worth noting that the range of maximum strain in the models was nearly identical and occurred at a distance of 400 to 800 mm from the slip direction.

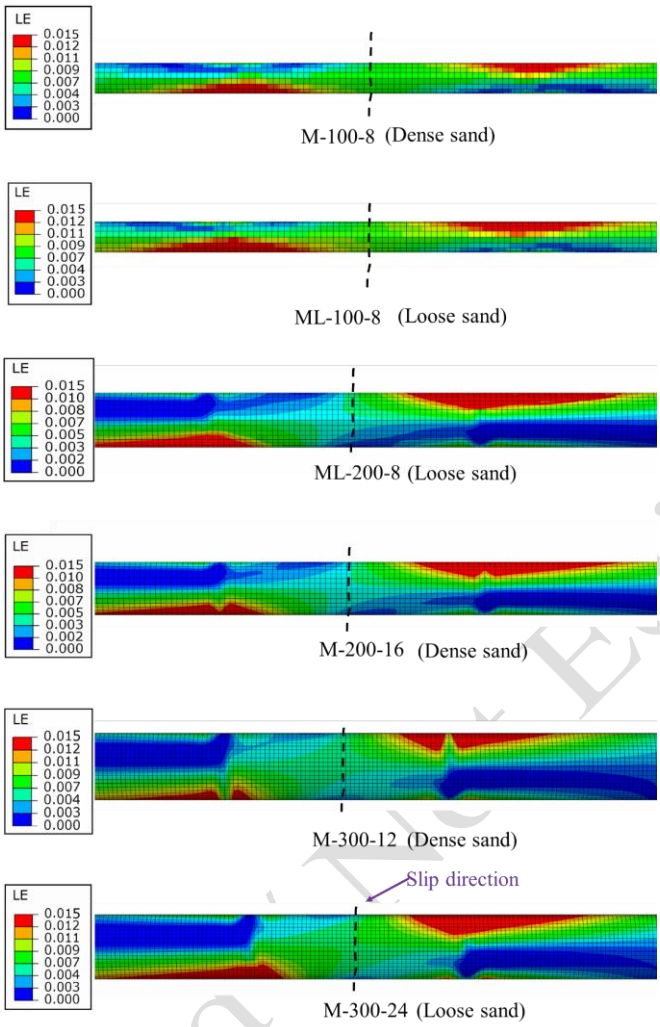

Fig. 13 The strain distribution of several models at the moment of failure.

According to the ASCE Guideline (2010), the maximum force applied per unit length of the pipe is determined using Eq. (1). In this equation, γ represents the soil density, and the parameter *Nqh* can be calculated based on the proposal by O'Rourke and Hansen (1999), as shown in Fig. 14. It is observed that the factor *Nqh* depends on the internal friction angle of the sand (ϕ) and the depth-to-diameter ratio of the pipe. The density and internal friction angle of dense sand were determined as 2220 kg/m³ and 40°, respectively, based on the conducted tests. The density and internal friction angle of loose sand were 1670 kg/m³ and 31°, respectively.

The objective of this section is to compare the maximum force results obtained from numerical analyses and the ASCE Guideline (2010). The maximum force applied to the pipe was calculated based on numerical analyses for a 4-meter section of the pipe. After determining the maximum force using Eq. (1) for the 4-meter, the results were compared

with those obtained from numerical models.

The numerical results revealed that pipe thickness had minimal influence on the maximum force in the pipe in loose sand, showing reasonable agreement with the ASCE Guideline results. Accordingly, the maximum pipe force results in loose sand were compared with the ASCE proposed Eq. (1). Conversely, the numerical results demonstrated that pipe thickness significantly affected the maximum force on the pipe in dense sand, with this effect becoming more pronounced as the pipe diameter increased. This behavior is attributed to the soil's resistance to penetration. In loose sand, due to low soil stiffness and high void ratio, the pipe penetrates and displaces the soil medium easily. Consequently, the resistance forces are low and independent of the pipe's thickness. In contrast, dense sand exhibits significant resistance to penetration due to high particle interlocking. The pipe cannot easily penetrate the soil, resulting in a stronger interaction where the pipe's thickness plays a critical role in overcoming the soil resistance and generating higher forces. Therefore, to align the results with the ASCE Guideline, Eq. (1) was modified into Eq. (2), where N'_{qh} was defined as shown in Eq. (3). A correction factor was introduced for Nqh, a dimensionless parameter dependent on pipe thickness. This equation was derived using the curve-fitting technique based on numerical results. Fig. 15 illustrates the maximum force results obtained from the numerical model and ASCE guidelines, represented by Eq. (1). As observed, the results for loose sand models exhibit acceptable accuracy.

$$P_u = \gamma \times D \times H \times N_{qh} \tag{1}$$

$$P_{u_D} = \gamma \times D \times H \times N'_{qh} \tag{2}$$

$$N'_{qh} = 85\left(\frac{D \times t}{H^2}\right)^{0.63} \times N_{qh} \tag{3}$$

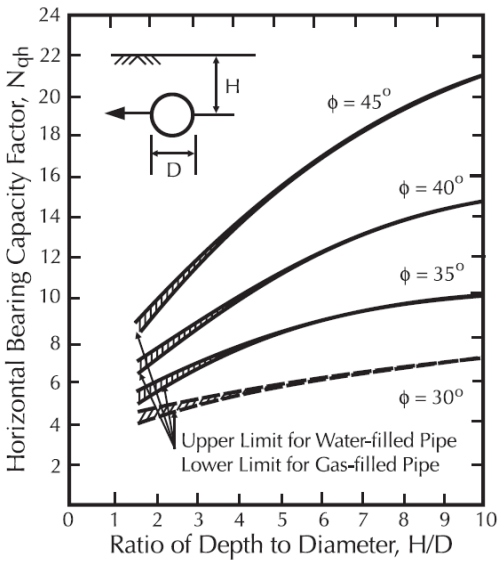

Fig. 14 The horizontal bearing capacity factor for sand relative to the depth-to-diameter ratio (O'Rourke and Liu, 1999)

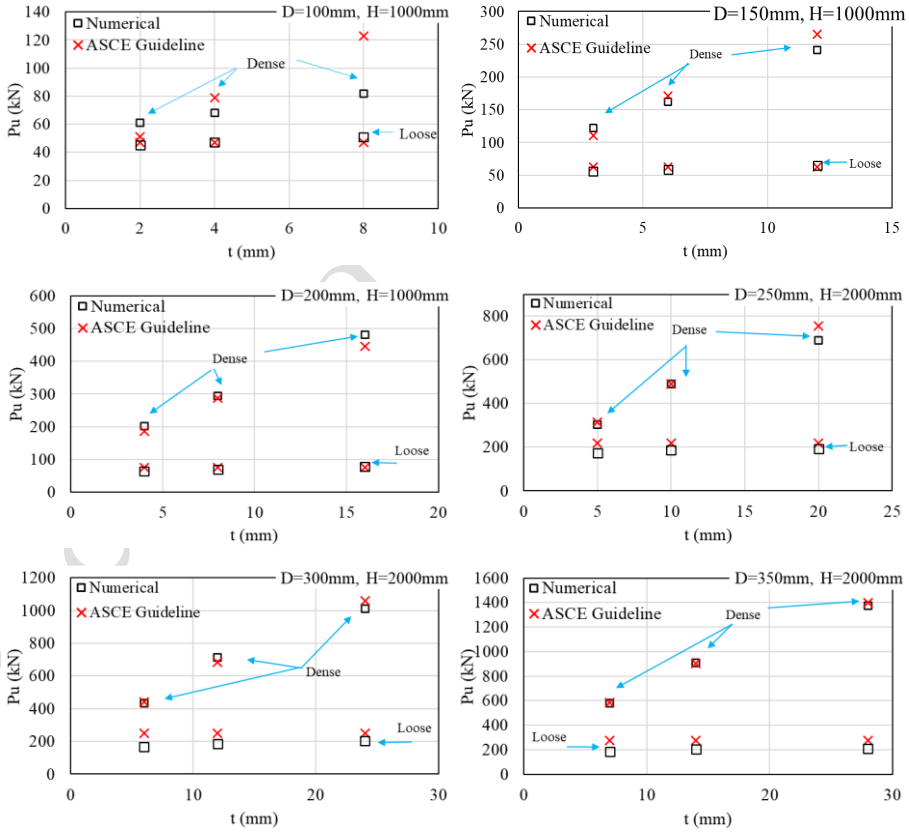

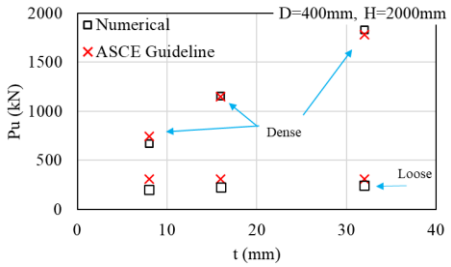

Fig. 15 Comparison of the maximum force results obtained from numerical models and ASCE Guideline (O'Rourke and Liu, 1999)

The numerical results for the maximum displacement of the pipe and the maximum force, as well as those obtained from Eqs. (1) and (2) are summarized in Table 8. Based on this table, it can be observed that the proposed equation (Eq. 2) yields results that closely match those of the numerical analyses.

Table 8 Results of numerical models

Models	Max Disp. (mm)		Force (kN)			
			Numerical		Analytical	
	L	D	L	D	L (Eq. 1)	D (Eq. 2)
M-100-2	187	83	45	61	47	51
M-100-4	191	85	47	68	47	79
M-100-8	201	95	51	82	47	123
M-150-3	236	164	56	122	63	111
M-150-6	243	172	59	162	63	171
M-150-12	260	189	65	241	63	265
M-200-4	272	252	65	202	76	186
M-200-8	289	253	70	295	76	287
M-200-16	309	286	79	481	76	445
M-250-5	351	291	173	304	220	316
M-250-10	370	305	188	490	220	489
M-250-20	395	319	194	690	220	756
M-300-6	387	336	167	435	250	442
M-300-12	407	355	184	714	250	685
M-300-24	441	368	203	1010	250	1060
M-350-7	409	377	185	581	278	585
M-350-14	430	390	203	909	278	905
M-350-28	466	408	208	1374	278	1400
M-400-8	433	406	202	672	306	743
M-400-16	450	423	228	1157	306	1150
M-400-32	489	441	242	1827	306	1779

The results of this study provide valuable insights for pipeline design in regions affected by fault rupture or seismic activity. The observed variations in pipe behavior between loose and dense sandy soils highlight the necessity of site-specific design considerations. Specifically, the greater displacement required for pipe failure in loose sand indicates that pipelines in such conditions may benefit from increased flexibility in their design to accommodate larger deformations without failure. On the other hand, pipelines in dense sand experience

concentrated deformation over shorter lengths, necessitating more robust reinforcement near the fault zones to mitigate the risk of localized damage.

Moreover, the significant influence of pipe diameter and thickness on the displacement and force characteristics underscores the importance of optimizing these parameters during the design phase. For pipelines with smaller diameters, the pronounced differences in displacement behavior between soil types suggest a need for more detailed soil-structure interaction analyses. Additionally, the modification of the ASCE guideline equation to account for pipe thickness ensures more accurate force predictions in dense sand, enabling engineers to design pipelines with improved resilience to fault-induced stresses. These findings serve as a foundation for developing more reliable and efficient pipeline systems in fault-prone areas.

6. Conclusion

In this study, the behavior of GRP pipes in dense and loose sandy soils under strike-slip fault conditions was investigated. Both experimental and numerical studies were conducted. Initially, four pipes with diameters of 100 and 200 millimeters were examined experimentally in dense and loose sand. Subsequently, the maximum forces and the absolute displacement of the pipe at the moment of failure were calculated. The numerical studies continued to evaluate the effects of pipe diameter and thickness on the deformation at the moment of failure, the location of maximum strain at the moment of failure, and the corresponding total force at pipe failure. Additionally, the maximum force results obtained from numerical models were compared with the proposed equation in the ASCE standard. The summary of the results is presented in the following points:

- Increasing the pipe diameter leads to a higher displacement required for pipe failure, with a more significant effect in dense sand. For example, the displacement ratio for D8 is 1.5 for ML-200/ML-100 and 2.9 for MD-200/MD-100.
- At pipe failure, the fixed section rapidly returned to its initial state, marked by a sharp drop in D4 displacement and applied force. Pipes with a 200 mm diameter showed greater displacements and more significant drops, making D4 displacement a reliable indicator for identifying the failure moment.
- The maximum logarithmic strain at pipe failure was found to be between 0.015 and 0.016 for all models, providing a consistent criterion for identifying the moment of

pipe failure.

- The numerical results showed that increased pipe diameter and thickness led to greater displacement required for pipe failure. Displacements at sections D6 to D8 were nearly identical across all models in dense and loose sand.
- The numerical results showed that displacement required for pipe failure was greater in loose sand than in dense sand. As pipe diameter decreased, the difference in displacement between the two sands became more pronounced. For example, model M-100-8 had a maximum displacement of 201 mm in loose sand and 94 mm in dense sand, a 113% increase. Conversely, model M-400-32 showed a smaller difference, with displacements of 489 mm in loose sand and 437 mm in dense sand, reflecting an 11% increase.
- The numerical results indicated that pipe thickness had a lesser effect on the maximum force of the pipe in loose sand, leading to good agreement with the results of the ASCE standard. In contrast, the maximum force in dense sand was significantly influenced by pipe thickness. Therefore, due to the absence of a thickness parameter in the proposed equation of the standard, a correction factor was defined to align its results with the numerical outcomes.

References

Aghazadeh K., Totonchi, B.A. and Attarnejad, R. (2025) A Comparative Study and Analysis of Transmission Vapor Pipelines for Optimizing Water Purification and Transfer. Civil Engineering Infrastructures Journal, -.10.22059/ceij.2025.392043.2273

Astm D. (2011) Standard test method for direct shear test of soils under consolidated drained conditions. D3080/D3080M, 3(9)

Chaudhuri C.H. and Choudhury, D. (2020) Buried pipeline subjected to seismic landslide: A simplified analytical solution. Soil Dynamics and Earthquake Engineering, 134, 106155.https://doi.org/10.1016/j.soildyn.2020.106155

Cheraghi K., Tahamouli Roudsari, M., Kiasat, S. and Esfandiari, J. (2024) Numerical and Analytical Study of the Cyclic Behavior of ADAS Damper and the Effect of Axial Force on its Behavior. Journal of Earthquake Engineering, 28(13), 3706-3723.https://doi.org/10.1080/13632469.2024.2345821

Cheraghi K. and Tahamouliroudsari, M. (2024) Numerical and analytical study of cyclic behavior of TADAS and the impact of axial force on its performance. Steel and Composite Structures, 53(2), 195-208.https://doi.org/10.12989/scs.2024.53.2.195

Dezhkam B. and Nouri, A.Z. (2018) Dynamic response of nanoparticle-water pipes buried in the soil subjected to far-fault earthquake using numerical method. Soil Dynamics and Earthquake Engineering, 113, 174-179.https://doi.org/10.1016/j.soildyn.2018.06.002

Engineers A. ASCE/SEI 7-10. American Society of Civil Engineers, 2010.

Hosseini M. and Roudsari, M.T. (2015) Minimum Effective Length and Modified Criteria for Damage Evaluation of Continuous Buried Straight Steel Pipelines Subjected to Seismic Waves. Journal of Pipeline Systems Engineering and Practice, 6(4), 04014018.https://doi.org/10.1061/(ASCE)PS.1949-1204.0000193

Kliszczewicz B. (2021) Analysis of the Pipelines Functional Safety on the Mining Areas. Periodica Polytechnica Civil Engineering, 65(4), 1126-1133.https://doi.org/10.3311/PPci.18639

Li H., Feng, X. and Zhao, L. (2022) Failure analysis of a buried large-diameter prestressed concrete cylinder pipeline subjected to strike-slip fault displacement. Tunnelling and Underground Space Technology, 121, 104334.https://doi.org/10.1016/j.tust.2021.104334

Liu J., Zhang, X., Li, L. and Saboundjian, S. (2018a) Resilient Behavior of Unbound Granular Materials Subjected to a Closed-System Freeze-Thaw Cycle. Journal of Cold Regions Engineering, 32(1), 04017015.https://doi.org/10.1061/(ASCE)CR.1943-5495.0000142

Liu X., Zhang, H., Xia, M., Chen, Y., Wu, K. and Wang, B. (2018b) Numerical Analysis and Strength Evaluation of an Exposed River Crossing Pipeline with Casing Under Flood Load. Periodica Polytechnica Civil Engineering, 62(4), 911-920.https://doi.org/10.3311/PPci.11605

O'rourke M.J. and Liu, X. 1999. Response of buried pipelines subject to earthquake effects, Mceer New York.

Ono K., Terada, K., Sawada, Y., Ling, H.I. and Kawabata, T. (2018) Fluid Coupled-DEM Simulation of Lateral Loading Experiment for Buried Pipe in Saturated Sand. Transportation Infrastructure Geotechnology, 5(2), 93-113.https://doi.org/10.1007/s40515-018-0050-5

Rasouli H. and Fatahi, B. (2020) Geofoam blocks to protect buried pipelines subjected to strike-slip fault rupture. Geotextiles and Geomembranes, 48(3), 257-274.https://doi.org/10.1016/j.geotexmem.2019.11.011

Song W.-K. (2006) Thermal Transfer Analysis of a Freezing Soil Medium with an Embedded Pipeline. Journal of Cold Regions Engineering, 20(1), 20-36.https://doi.org/10.1061/(ASCE)0887-381X(2006)20:1(20)

Soveiti S. and Mosalmani, R. (2020) Mechanical behavior of buried composite pipelines subjected to strike-slip fault movement. Soil Dynamics and Earthquake Engineering, 135, 106195.https://doi.org/10.1016/j.soildyn.2020.106195

Tahamouli Roudsari M., Hosseini, M., Ashrafy, M., Azin, M., Nasimi, M., Torkaman, M. and Khorsandi, A. (2022) New Method to Evaluate the Buried Pipeline– Sandy Soil Interaction Subjected to Strike Slip Faulting. Journal of Earthquake Engineering, 26(1), 89-112.https://doi.org/10.1080/13632469.2019.1662343

Tahamouli Roudsari M., Samet, S., Nuraie, N. and Sohaei, S. (2017) Numerically Based Analysis of Buried GRP Pipelines under Earthquake Wave Propagation and Landslide Effects. Periodica Polytechnica Civil Engineering, 61(2), 292-299.https://doi.org/10.3311/PPci.9339

Talebi F. and Kiyono, J. (2020) Introduction of the axial force terms to governing equation for buried pipeline subjected to strike-slip fault movements. Soil Dynamics and Earthquake Engineering, 133, 106125.https://doi.org/10.1016/j.soildyn.2020.106125

Thang V., Hui, D., Marshall, P.W. and Zhou, J. (2022) Performance of steel–polymer–steel seafloor pipeline buried in earthquake fault zones. Archives of Civil and Mechanical Engineering, 22(4), 174.https://doi.org/10.1007/s43452-022-00495-5

Triantafyllaki A., Papanastasiou, P. and Loukidis, D. (2021) Offshore pipeline performance under strike-slip fault movements. Soil Dynamics and Earthquake Engineering, 147, 106698.https://doi.org/10.1016/j.soildyn.2021.106698

Vazouras P., Dakoulas, P. and Karamanos, S.A. (2015) Pipe–soil interaction and pipeline performance under strike–slip fault movements. Soil Dynamics and Earthquake Engineering, 72, 48-65.https://doi.org/10.1016/j.soildyn.2015.01.014

Wang Z., Lu, Z., Zhang, D. and Liu, H. (2020) Stress effect of the interface between buried pipeline and sandy soil layer in a cold environment. Cold Regions Science and Technology, 172, 102981.https://doi.org/10.1016/j.coldregions.2019.102981

Xu G., Cai, L., Ji, R. and Wang, Z. (2018) Numerical simulation of pipe-soil interaction during pulling back phase in horizontal directional drilling installations. Tunnelling and Underground Space Technology, 76, 194-201.https://doi.org/10.1016/j.tust.2018.03.022

Zhang W. and Askarinejad, A. (2019) Behaviour of buried pipes in unstable sandy slopes. Landslides, 16(2), 283-293.https://doi.org/10.1007/s10346-018-1066-1

Zhu J., Pan, J., Zhang, Y., Li, Y., Li, H., Feng, H., Chen, D., Kou, Y. and Yang, R. (2023) Leakage and diffusion behavior of a buried pipeline of hydrogen-blended natural gas. International Journal of Hydrogen Energy, 48(30), 11592-11610.https://doi.org/10.1016/j.ijhydene.2022.10.185